Lawrence Berkeley National Laboratory
Applied Math & Comp Sci

Title

Multiscale Modeling of Membrane Rearrangement, Drainage, and Rupture in Evolving Foams

Permalink

https://escholarship.org/uc/item/7442z88n

Journal

Science, 340(6133)

ISSN

0036-8075

Authors

Saye, Robert I
Sethian, James A

Publication Date

2013-05-10

DOI

10.1126/science.1230623

Peer reviewed

7. J. A. Fan et al., Science 328, 1135 (2010).
8. A. R. Schmidt et al., Nature 465, 570 (2010).
9. M. Kroner et al., Nature 451, 311 (2008).
10. A. E. Miroshnichenko, S. Flach, Y. S. Kivshar, Rev. Mod. Phys. 82, 2257 (2010).
11. S. H. Linn, W.-B. Tzeng, J. M. Brom, C. Y. Ng, J. Chem. Phys. 78, 50 (1983).
12. Materials and methods are available as supplementary materials on Science Online.
13. D. Riffe, Phys. Rev. B 84, 064308 (2011).
14. C. Szymanowski, C. H. Keitel, B. J. Dalton, P. L. Knight, J. Mod. Opt. 42, 985 (1995).
15. P. B. Corkum, F. Krausz, Nat. Phys. 3, 381 (2007).
16. C. Ott et al., http://arxiv.org/abs/1205.0519 (2012).
17. K. Ito, K. Yoshino, Y. Morioka, T. Namioka, Phys. Scr. 36, 88 (1987).
18. M. Chini et al., Phys. Rev. Lett. 109, 073601 (2012).
19. R. Shakhmuratov, F. Vagizov, O. Kocharovskaya, Phys. Rev. A 84, 043820 (2011).
20. S. E. Harris, Phys. Today 50, 36 (1997).
21. A. H. Safavi-Naeini et al., Nature 472, 69 (2011).
22. O. Kocharovskaya, Phys. Rep. 219, 175 (1992).
23. M. O. Scully, Phys. Rep. 219, 191 (1992).
24. J. Herrmann et al., http://arxiv.org/abs/1206.6208 (2012).
25. P. Lambropoulos, P. Zoller, Phys. Rev. A 24, 379 (1981).
26. Z. H. Loh, C. H. Greene, S. R. Leone, Chem. Phys. 350, 7 (2008).
27. S. Gilbertson et al., Phys. Rev. Lett. 105, 263003 (2010).
28. H. Wang et al., Phys. Rev. Lett. 105, 143002 (2010).
29. W.-C. Chu, C. D. Lin, Phys. Rev. A 87, 013415 (2013).

Multiscale Modeling of Membrane Rearrangement, Drainage, and Rupture in Evolving Foams

Robert I. Saye[1] and James A. Sethian[1]*

Modeling the physics of foams and foamlike materials, such as soapy froths, fire retardants, and lightweight crash-absorbent structures, presents challenges, because of the vastly different time and space scales involved. By separating and coupling these disparate scales, we have designed a multiscale framework to model dry foam dynamics. This leads to a predictive and flexible computational methodology linking, with a few simplifying assumptions, foam drainage, rupture, and topological rearrangement, to coupled interface-fluid motion under surface tension, gravity, and incompressible fluid dynamics. Our computed results match theoretical analyses and experimentally observed physical effects, including thin-film drainage and interference, and are used to study bubble rupture cascades and macroscopic rearrangement. The developed multiscale model allows quantitative computation of complex foam evolution phenomena.

O ne of the hallmarks of natural phenomena is that they often occur across multiple space and time scales. An example comes from climate studies, in which oceanic and atmospheric waves spanning hundreds of kilometers are influenced by temperature variations in localized environments. In such "multiscale problems," the unfolding of small-scale processes, depending on physics, chemistry, and biology, combine to produce large-scale effects, and these macroscopic dynamics subsequently affect the interplay of microscopic forces. Traditionally, computational models rely on accurately modeling the smallest possible space and time scales. However, in a multiscale problem, this technique may require such a fine resolution that there is no practical hope of following a calculation long enough to observe the macroscale behavior, even with today's advanced computing hardware.

Fortunately, the details at one space or time scale are not necessarily important at another scale. By devising different models and equations at different scales, we can "separate scales" and compute physics at different resolutions, allowing these different models to communicate across the scales. The challenge is to find such a scale separation and develop models that are computationally tractable, so that critical information is communicated between scales without creating artificial physics.

An everyday example of multiscale physics can be found in foams, which have a wide variety of applications in industry and materials design. Liquid foams, characterized by fluid-filled membranes separating gaseous regions, include soapy detergents, substances to separate out hydrophobic molecules, and even the head on a beer. Solid foams, formed by solidifying liquid foams, include lightweight materials such as metallic and plastic foams. Understanding the dynamics of foam evolution is a key step in controlling the structure and properties of foamlike materials. Deriving models to quantitatively predict foam evolution is challenging because the underlying physics takes place over vastly different time and space scales.

In this work, we use a foam of common soap bubbles as our prototypical example. A single bubble consists of a thin membrane of fluid, known as the lamella, separating the inside gas from the outside. In a cluster of such bubbles (Fig. 1A), multiple lamellae meet at junctions called Plateau borders, forming a network of interconnected thin-film membranes. The dynamics of this foam cluster are intricate (1) and depend on a complex interaction between microscale fluid flow inside the lamellae and Plateau borders, and the macroscale motion of the gas inside the bubbles. To illustrate, consider a foam whose macroscopic configuration appears to be in equilibrium, such as the foam in Fig. 1A. Although seemingly stable, liquid inside the films drains over time, owing to effects of gravity and surfactant. When one of the membranes becomes too
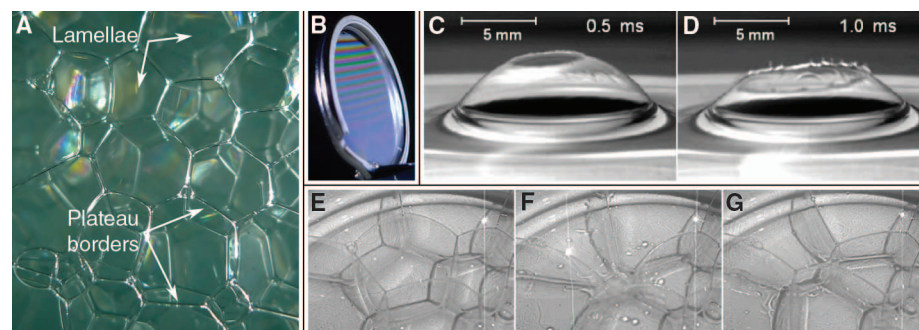

Fig. 1. Physics of foam drainage. (**A**) A foam of soap bubbles made with common washing detergent. (**B**) Drainage and thin-film interference. A keyring suspended in soap solution makes a film, which then drains owing to gravity. The subsequent variations in film thickness create interference patterns when lit with white light. (**C** and **D**) Rupture of a lamella. [Reproduced from (2) by permission from Macmillan Publishers Ltd, Nature, copyright 2010] (**E** to **G**) Rearrangement. A lamella [center of (E)] bursts, leading to macroscopic rearrangement of a foam.

[1]Department of Mathematics and Lawrence Berkeley National Laboratory, University of California, Berkeley, CA 94720, USA.

*Corresponding author. E-mail: sethian@math.berkeley.edu

thin, it ruptures and its liquid contents are re-distributed, destroying the macroscopic equilibrium of the remaining membranes. Driven by macroscale gas dynamics and surface tension, these other membranes, as well as their film thicknesses, further change as they contort, stretch, and settle into a new equilibrium, setting the stage for continued fluid drainage.

These processes take place over six orders of magnitude in space and time. The liquid in the thin films, though only micrometers thick, drains over tens or hundreds of seconds (Fig. 1B) until a membrane ruptures (Fig. 1, C and D). Membranes burst at hundreds of centimeters per second (2), causing macroscopic rearrangement of bubble topology through surface and fluid forces occurring over less than a second (Fig. 1, E to G). Considerable mathematical analyses, as well as numerical and experimental studies, have focused on these individual components. These include studying the geometry of stable foams—for example, in Plateau's laws (3)—and computational methods to find minimal surfaces (4, 5); evolutionary laws for foam geometry, such as the two-dimensional (2D) von Neumann–Mullins law (6, 7), its extension to three dimensions (8), and statistical variations (9); thin-film equations for drainage in stationary films (10, 11), as well as drainage equations in stationary networks of Plateau borders (12); and experimental studies of topological changes in 2D foams (13). In addition, computational tools aimed at specific aspects of macroscopic rearrangement include numerical studies of multiphase fluid flow separated by massless and infinitely thin interfaces that do not drain or rupture (14, 15); foam studies based on 2D hydrodynamics (16); and contributions made by the Surface Evolver software (17) in computing minimal energy states of complex configurations.

Here, we exploit the idea of scale separation to introduce a multiscale model that separates foam dynamics into a cycle of three distinct stages, coupling different scales across space and time. These stages are (i) a rearrangement phase, in which a foam out of macroscopic balance undergoes rearrangement due to surface tension and gas dynamics, leading to an equilibrium; (ii) a liquid drainage phase, in which the foam is essentially in macroscopic equilibrium, and the microscopic flow of liquid is modeled until a lamella becomes too thin; and then (iii) a rupture phase, in which a lamella ruptures, sending the foam out of macroscopic balance, after which step (i) is invoked and the process repeated. Together, the dynamics of each phase affects the next, leading to a multiscale model that captures the key effects of foam rearrangement, liquid drainage, and rupture.

Our scale-separated model assumes that the gas and liquid flow are incompressible within the time and space scales under consideration; liquid evaporation in the lamellae occurs during a longer time scale than rearrangement, drainage, and rupture; and the liquid-gas interface has a no-slip boundary condition with a uniformly constant surface tension. Additional forces, scales, and regimes, beyond those included here, play an important role in foam dynamics, although they can be added to this framework. Diffusive coarsening, which results from gas exchange between bubbles separated by permeable membranes, is important over very long time scales (minutes to hours) (1); although our macroscale Navier-Stokes fluid solver easily allows such permeability effects, our thin-film equations are derived assuming a static equilibrium, and thus we do not not include coarsening effects. At the liquid-gas interface, we idealize that Marangoni forces, which act to equilibrate surfactant concentration, occur quickly enough to produce a uniformly constant surface tension, while the no-slip boundary condition assumption ignores some effects of surface rheology, which can be important for surfactant solutions exhibiting mobile boundary conditions. Finally, we focus on dry foams [i.e., foams with liquid occupying less than ~10% of the total volume (1)], though the methodology below has extensions to wet foam modeling as well.

Turning to the individual phases, consider first the rearrangement phase, in which the foam structure is out of macroscopic equilibrium. Surface tension at the liquid-gas interface influences
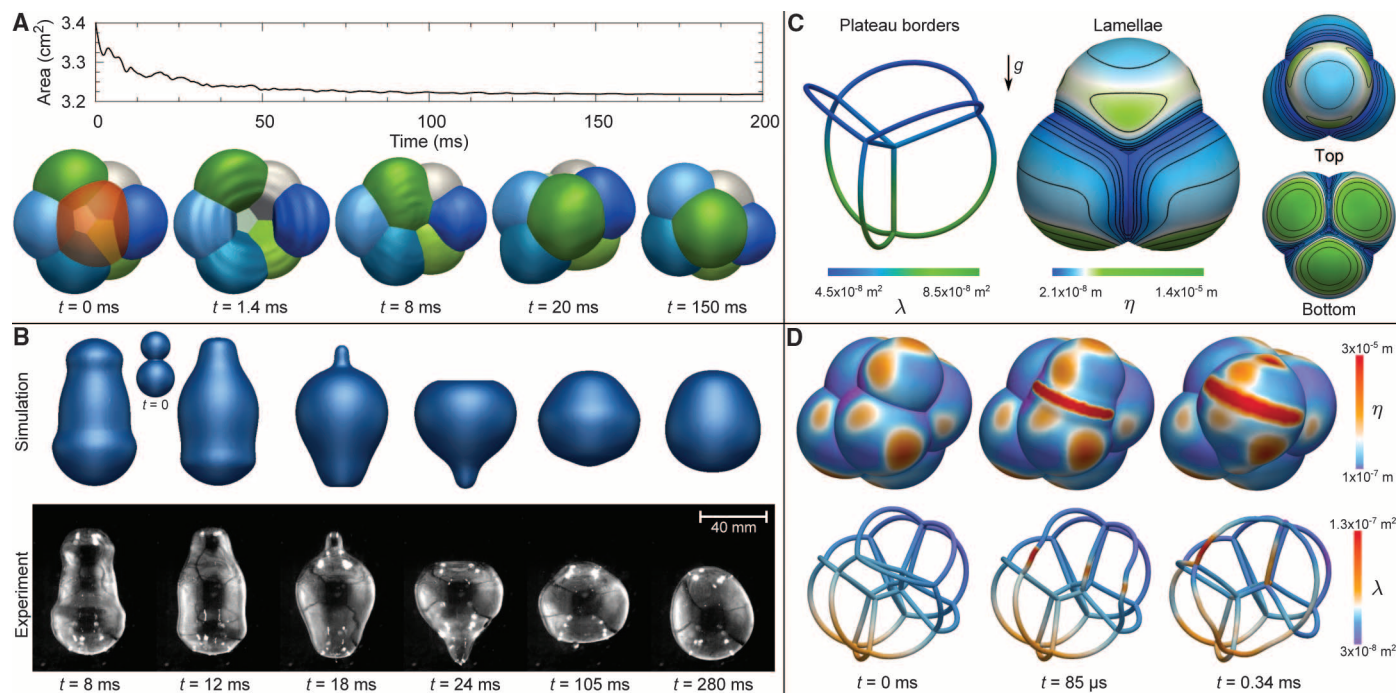
Fig. 2. Verification of numerical methodology. (**A**) A small cluster, initially in equilibrium, undergoes rearrangement due to the removal of a lamella (orange) at time *t* = 0. Total surface area of the cluster is shown in the plot; see also movie S1. (**B**) Comparison of numerical results with experiment. Two spherical soap bubbles merge at *t* = 0, subsequently causing surface-tension–driven oscillations that eventually lead to a larger spherical bubble. [Experimental results reproduced from (23) by permission of IOP Publishing] Numerical simulation uses identical physical parameters and time scale (see table S1). (**C**) Solution of the coupled lamella and Plateau border thin-film equations on a pyramid of spherical bubbles. Colors indicate thickness η of the lamella and cross-sectional area λ of the Plateau border, and the black lines are contour lines of η. (**D**) Evolution during rupture. An internal lamella joining the two front facing bubbles ruptures and is removed, leading to rearrangement of bubbles and varying film thicknesses; see movie S2 for an animated view.

the gas dynamics, which in turn evolve the network of lamellae and Plateau borders, rearranging the system of bubbles. Liquid contained in the thin films and Plateau borders is conserved and transported during this readjustment. Because macroscopic fluid mechanics determine the motion, we idealize the membranes as massless and vanishingly thin, thereby approximating their inertial effects as negligible. Mathematically, this leads to the incompressible Navier-Stokes equations for the gas phase, with continuity of the velocity field across the liquid-gas interface Γ, and an effective surface tension of 2σ (i.e., twice the coefficient of a single liquid-gas interface). The interface is thus advected by the velocity field **u** of the gas, satisfying

$$\rho_g(\mathbf{u}_t + \mathbf{u} \cdot \nabla \mathbf{u}) = -\nabla p + \mu_\mathbf{g}\Delta \mathbf{u} - 2\sigma\kappa\mathbf{n}\delta_\varepsilon(\Gamma)$$

where μ_g is the viscosity of the gas and ρ_g is its density. We have implemented surface tension with a continuum approach (18, 19), whereby the force, existing only at the interface, becomes a body force $2\sigma\kappa\mathbf{n}\delta_\varepsilon(\Gamma)$ through the use of a smoothed Dirac delta function with support concentrated at the interface. The resulting dynamics naturally enforce 120° angle conditions at Plateau borders obeyed by dry foams and allow the interface to change topology (14, 15).

During rearrangement, the liquid in the lamellae and Plateau borders is transported by the motion of the interface in such a way that the amount of liquid is locally conserved. We exploit the thinness of the lamellae and Plateau borders by describing their "thickness" with a scalar function, allowed to vary in space and time. For the lamella, its half-thickness is defined as η, and for the Plateau border, we define λ as the cross-sectional area at any particular location in space; see fig. S1. For liquid contained in the lamellae, conservative transport is modeled by requiring that

$$\frac{d}{dt}\int_{S(t)} \eta = 0$$

where $S(t)$ is any surface patch on $\Gamma(t)$ passively advected by the velocity field **u**. This model conserves the mass of liquid in the lamellae by measuring the amount of stretching in the interface, and it allows surface currents at the interface to move the liquid tangentially. Liquid in the Plateau borders is conserved with an analogous conservation law.

During the liquid drainage phase, the foam is essentially in macroscopic equilibrium, which means that the dynamics of the gas phase may be taken as negligible, and the surface area has been locally minimized, hence individual lamella have constant mean curvature. We thus require a model for liquid drainage in the (fixed) network of lamellae and Plateau borders. By capitalizing on the inherent scales involved and following the philosophy of "thin-film approximations" (10, 11), which describe the evolving membrane thickness in a single lamella, we build thin-film approximations for drainage in the curved lamellae, as well as the Plateau borders, and devise inter-

related boundary conditions that couple the regions together.

For a lamella of constant mean curvature, we have the partial differential equation (PDE) (see the supplementary online text for further details on the derivation),

$$\eta_t + \frac{1}{3\mu}\nabla_s \cdot \left(\sigma\eta^3\nabla_s((k_1^2 + k_2^2)\eta + \Delta_s\eta) + \rho\mathbf{g}_s\eta^3\right) = 0$$

where μ is the viscosity of the liquid, ρ is its density, and $\mathbf{g}_s$ is the component of gravity tangential to the surface. Here, ∇_s is the surface gradient, $\nabla_s \cdot$ is the surface divergence, and Δ_s is the surface Laplacian on the curved surface of the lamella, while k_1 and k_2 are its principal curvatures. This is a fourth-order PDE and needs two boundary conditions on the boundary of the lamella. One condition is chosen to be that of zero Neumann: $\partial\eta/\partial\nu = 0$, where ν is tangent to the lamella and orthogonal to its boundary. The other is provided by a flux boundary condition (20, 21) that implements suction of liquid into the Plateau borders at its boundary. The amount of flux is determined by matching the thickness of the lamella to the cross-sectional curvature of the Plateau border under a local Stokes flow argument. In this model, we include effects of surface tension, the curved surface of the lamella, and gravity. Additional physics, such as dis-

joining pressure and van der Waals forces, which are important for films exhibiting long lifetimes, fits into our model by suitably modifying the PDE.

A similar PDE is derived for the thickness of a Plateau border

$$\lambda_t + \frac{C_\Delta}{\mu}\frac{\partial}{\partial l}\left(-\frac{1}{2}(\sqrt{3} - \frac{\pi}{2})^{1/2}\sigma\lambda^{1/2}\partial_l\lambda + \lambda^2\rho g_\tau\right) = S$$

where C_Δ is a constant associated with the cross-sectional shape of the Plateau border, g_τ is the tangential component of gravity, and S is a source term representing the incoming liquid from the three lamellae connected to the Plateau border. This equation requires boundary conditions where Plateau borders meet at quadruple junctions, and these are provided by conservation of liquid mass and quasi-static pressure balance.

The rupture phase occurs when a lamella becomes critically thin as a result of drainage. A small tear appears, and the hole in this curved 2D sheet rapidly expands as surface tension causes the membrane to retract. For the bubble sizes considered here, liquid in the membrane retreats to the Plateau borders (2), and this occurs over a time scale that is just a small fraction of the total time it takes for bubbles to rearrange. Although this rupture could itself be treated as an evolving interface within our algorithmic framework, albeit with a more restrictive time-step
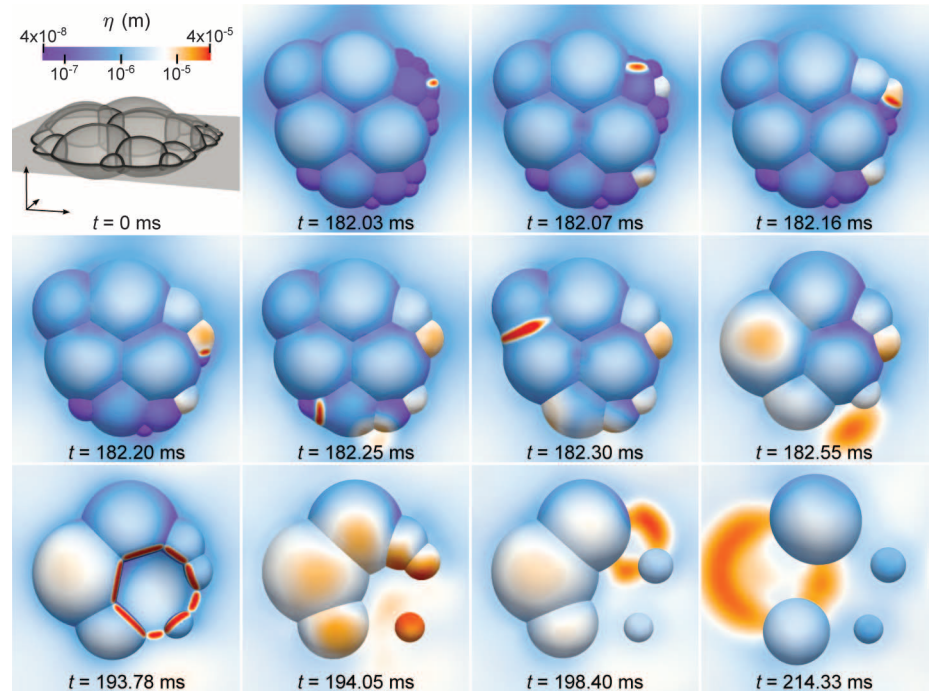

Fig. 3. Results of the coupled multiscale model for a cluster of bubbles attached to a membrane. In the top-left frame, a side view of the initial configuration is shown, using semi-opaque lamellae and emphasizing the Plateau borders, to highlight the 3D structure of the results. In the rest of the frames, a top-down view is given, showing the lamellae film thickness η, corresponding to the indicated color scale. The background membrane absorbs some of the drainage, but is chosen not to rupture. As the system evolves, rupture events can be identified by the localized increases in lamellae thickness. (See movie S3 for the complete simulation.)

requirement in the numerical calculation, we simplify and assume that rupture, once initiated through a prescribed threshold, is instantaneous and that liquid in a ruptured lamella is uniformly distributed to the neighboring Plateau borders.

We now introduce a collection of numerical technologies to accurately compute the solution of these coupled scale-separated equations; more details are given in (19). We solve the incompressible Navier-Stokes equations using a finite difference method implemented on a fixed Eulerian grid, together with a projection method (22) that uses a type of Hodge decomposition to enforce incompressibility when updating the velocity field. The interfaces are tracked with the "Voronoi Implicit Interface Method (VIIM)" (14, 15), which alternates between a finite-difference PDE level set advancement of a single unsigned distance function and a geometric Voronoi reconstruction step, and robustly captures topological change, including transitions at multiple junctions.

To solve the thin-film flow equations, we discretize (i) lamellae as a collection of connected triangulated manifolds, constructed with a new meshing algorithm devised to produce high-quality triangulations, and (ii) the Plateau borders as a network of connected line segments at the junctions of the mesh; see fig. S2. Within each, we design a finite element method to approximate the equations in weak form, using a biharmonic-modified forward time-stepping scheme that ameliorates time-step constraints typically associated with fourth-order nonlinear PDEs. The solutions from the individual lamellae and Plateau borders are coupled together though discretized forms of the flux and quadruple-point boundary conditions. Finally, rupture occurs when the film thickness falls below a chosen minimum value, followed by the macroscopic rearrangement phase.

Before applying our framework to modeling the complete system, we first test and verify individual components, using physical parameters corresponding to a typical gas and typical soap solution; precise values are given in table S1.

We first consider a cluster of bubbles, initially in equilibrium, and then remove a specific lamella (Fig. 2A). After removal, surface tension drives the cluster into a new configuration, undergoing various topological changes in the process. Figure 2A (top) plots the total surface area as a function of time and shows that it reaches a local minimum; Fig. 2A (bottom) (see also movie S1) illustrates how the "hole" made by removing the lamella is filled in, generating capillary waves as it does so, with 120° angle conditions satisfied throughout the process, ultimately leading to an equilibrium where each lamella has constant mean curvature.

To test the accuracy of our Navier-Stokes solver, we compared numerical results with that of an experiment (23), whereby two spherical soap bubbles merge into one bubble, causing surface-tension–driven oscillations (Fig. 2B). Good agreement between the numerical model and experiment is obtained.

Next, we verify that our finite element thin-film equation solvers correctly model liquid drainage (Fig. 2C). A pyramid of four spheres forms a network of six lamellae and 10 Plateau borders. The lamellae are initialized at time $t = 0$ with a uniform thickness of $\eta = 5$ μm and the Plateau borders with uniform cross-sectional area $\lambda = 0.05$ mm^2. Figure 2C shows the thickness after draining for 16.1 s. The effect of gravity is seen with the accumulation of liquid at the bottom of the lamellae and Plateau borders, while the effect of the flux boundary condition can be observed with the reduced thickness of the lamellae at the junctions.

To demonstrate rupture and redistribution of liquid mass, in Fig. 2D, a cluster of bubbles with nonuniform thickness has been draining, and the internal lamella separating the two front-facing bubbles ruptures immediately after time $t = 0$. The liquid originally contained in the lamella, together with the Plateau borders it was once connected to, is locally distributed to the remaining lamellae, as shown by the sudden increase in thickness. The system, driven by macroscopic rearrangement, quickly moves into a new configuration.

We now turn to the complete physical system, and use the multiscale model to predict the evolution of foam cluster dynamics under the combined effects of rearrangement, drainage, and rupture. In the first example, suppose that the lamellae start with a uniform thickness of η_0. Scaling arguments (see supplementary online text) applied to the lamella thin-film equation together with the flux boundary condition, suggest that the lamellae thicknesses develop a boundary layer, whose width after a fixed amount of time is $\mathcal{O}(\eta_0^{1/2}\lambda_0^{1/4})$, where λ_0 is a typical thickness of the Plateau border. For typical film thicknesses and drainage times, the length predicted by the scaling is on the order of 0.1 mm and was confirmed by numerical tests, as is the result that Plateau borders tend to have the same order of magnitude thickness across the entire network. It follows that for a cluster of bubbles that initially have the same lamellae thickness, all lamellae drain at approximately the same rate, and thus those bubbles smaller than the boundary layer will thin more rapidly and rupture first.

To demonstrate this behavior, and how it effects rearrangement of bubbles, an example is shown in Fig. 3 (see also movie S3 and table S1 for additional details). A cluster of 17 bubbles is suspended by a membrane, so that bubbles protrude below and above the membrane. We designed this configuration in order to make the rearrangement simpler to visualize with a top-down perspective. The cluster has a range of bubble sizes, from 0.1 to 0.5 mm in diameter, and at time $t = 0$ is initially in equilibrium, such that each lamella has a uniform thickness of 10 μm, and each Plateau border a uniform cross-sectional area of 0.002 mm^2. After draining for a time of 182 ms, some of the smallest lamellae rupture in quick succession. As this occurs, adjacent bubbles grow in size and increase in thickness. Initially, much of the rupture events are associated with the smaller lamellae, but because rupture affects the macroscopic dynamics of the bubbles, in some cases, larger lamellae rupture as a result of membrane stretching. On this small spatial scale, the rearrangement phase typically takes 0.1 ms to equilibrate, whereas drainage steps takes tens of milliseconds. The results show how a nontrivial sequence of rupture events is obtained, in that bubble rearrangement affects rupture events, both locally and globally, owing to changes in film thickness and macroscopic hydrodynamics.

In another example, we consider a cluster of 27 bubbles, with a larger typical bubble diameter
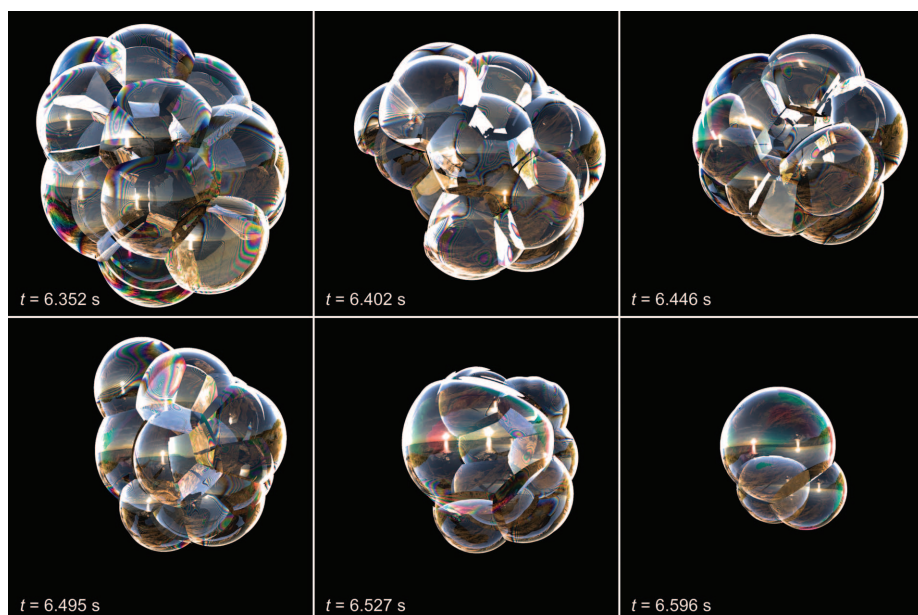

Fig. 4. Collapse of a foam cluster. Results shown with physically accurate thin-film interference, using a beach scene to provide environment lighting. (See movie S4 for the complete simulation.)

t = 6.352 s *t* = 6.402 s *t* = 6.446 s *t* = 6.495 s *t* = 6.527 s *t* = 6.596 s

of 3 mm (Fig. 4; see also movie S4). In the figures, thin-film interference is used to show the evolution, by using the lamellae thickness η to solve the Fresnel equations that determine the constructive and destructive interference of reflected light. After draining for 6.4 s, a single bubble bursts, which causes a rapid collapse of the foam structure. Compared to the case in Fig. 3, in this example the typical bubble size is much larger, which makes a priori prediction of rupture events less predictable.

In this work, we have developed a multiscale model of the interplay between gas, liquid, and interface forces for a dry foam, permitting the study of the effects of fluid properties, topology, bubble shape, and distribution on drainage, rupture, and rearrangement. We demonstrated the model by analyzing cascading properties of bubble rupture together with large-scale hydrodynamics. Both the scale-separated model and the underlying numerical algorithms are general enough to allow extension of the physics at individual scales to include other phenomena, such as disjoining pressure, diffusive coarsening, and different types of surface rheology, including liquid-gas interfaces with mobile/stress-free boundary conditions, surface viscosity, evaporation dynamics, and heating. The multiscale modeling and numerical methodologies presented here suggest a wide variety of related applications, such as in plastic and metal foam formation.

References and Notes
1. D. L. Weaire, S. Hutzler, *The Physics of Foams* (Oxford Univ. Press, 2001).
2. J. C. Bird, R. de Ruiter, L. Courbin, H. A. Stone, *Nature* **465**, 759 (2010).
3. J. Plateau, *Statique expérimentale et théorique des liquides soumis aux seules forces moléculaires* (Gauthier-Villars, Trubner et cie., Paris, France, 1873).
4. D. L. Chopp, *J. Comput. Phys.* **106**, 77 (1993).
5. K. Polthier, *Global Theory of Minimal Surfaces, Proceedings of the Clay Mathematics Institute 2001 Summer School*, D. Hoffman, Ed. (American Mathematical Society, Providence, RI, 2005).
6. J. von Neumann, *Metal Interfaces*, C. Herring, Ed. (American Society for Metals, Cleveland, OH, 1952), pp. 108–110.
7. W. W. Mullins, *J. Appl. Phys.* **27**, 900 (1956).
8. R. D. MacPherson, D. J. Srolovitz, *Nature* **446**, 1053 (2007).
9. S. Hilgenfeldt, A. M. Kraynik, S. A. Koehler, H. A. Stone, *Phys. Rev. Lett.* **86**, 2685 (2001).
10. A. Oron, S. H. Davis, S. G. Bankoff, *Rev. Mod. Phys.* **69**, 931 (1997).
11. T. G. Myers, *SIAM Rev.* **40**, 441 (1998).
12. S. A. Koehler, S. Hilgenfeldt, H. A. Stone, *J. Colloid Interface Sci.* **276**, 420 (2004).
13. M. Durand, H. A. Stone, *Phys. Rev. Lett.* **97**, 226101 (2006).
14. R. I. Saye, J. A. Sethian, *Proc. Natl. Acad. Sci. U.S.A.* **108**, 19498 (2011).
15. R. I. Saye, J. A. Sethian, *J. Comput. Phys.* **231**, 6051 (2012).
16. Y. Kim, M.-C. Lai, C. S. Peskin, *J. Comput. Phys.* **229**, 5194 (2010).
17. K. Brakke, *Exp. Math.* **1**, 141 (1992).
18. J. U. Brackbill, D. B. Kothe, C. Zemach, *J. Comput. Phys.* **100**, 335 (1992).
19. See supplementary materials on *Science* Online.
20. C. J. W. Breward, P. D. Howell, *J. Fluid Mech.* **458**, 379 (2002).
21. P. D. Howell, H. A. Stone, *Eur. J. Appl. Math.* **16**, 569 (2005).
22. A. J. Chorin, *Math. Comput.* **22**, 745 (1968).
23. U. Kornek *et al.*, *New J. Phys.* **12**, 073031 (2010).

Supplementary Materials
www.sciencemag.org/cgi/content/full/340/6133/720/DC1
Materials and Methods
Supplementary Text
Figs. S1 to S5
Table S1
References (*24–27*)
Movies S1 to S4

Spin-Optical Metamaterial Route to Spin-Controlled Photonics

Nir Shitrit, Igor Yulevich, Elhanan Maguid, Dror Ozeri, Dekel Veksler, Vladimir Kleiner, Erez Hasman*

Spin optics provides a route to control light, whereby the photon helicity (spin angular momentum) degeneracy is removed due to a geometric gradient onto a metasurface. The alliance of spin optics and metamaterials offers the dispersion engineering of a structured matter in a polarization helicity–dependent manner. We show that polarization-controlled optical modes of metamaterials arise where the spatial inversion symmetry is violated. The emerged spin-split dispersion of spontaneous emission originates from the spin-orbit interaction of light, generating a selection rule based on symmetry restrictions in a spin-optical metamaterial. The inversion asymmetric metasurface is obtained via anisotropic optical antenna patterns. This type of metamaterial provides a route for spin-controlled nanophotonic applications based on the design of the metasurface symmetry properties.

Metamaterials are artificial matter structured on a size scale generally smaller than the wavelength of external stimuli that enables a custom-tailored electromagnetic response of the medium and functionalities such as negative refraction (*1*), imaging without an intrinsic limit to resolution (*2*), invisibility cloaking (*3*), and giant chirality (*4*, *5*). An additional twist in this field originates from dispersion-engineered metamaterials (*6*, *7*). A peculiar route to modify the dispersion relation of an anisotropic inhomogeneous metamaterial is the spin-orbit interaction (SOI) of light; that is, a coupling of the intrinsic angular momentum (photon spin) and the extrinsic momentum (*8–10*). Consequently, the optical spin provides an additional degree of freedom in nano-optics for spin degeneracy removal phenomena such as the spin Hall effect of light (*9*, *11–14*). The chiral behavior originates from a geometric gradient associated with a closed loop traverse upon the Poincaré sphere generating the geometric Pancharatnam-Berry phase (*15*, *16*), not from the intrinsic local chirality of a meta-atom (*4*, *5*, *17*). Specifically, spin optics enables the design of a metamaterial with spin-controlled modes, as in the Rashba effect in solids (*18–21*).

The Rashba effect is a manifestation of the SOI under broken inversion symmetry [i.e., the inversion transformation $\mathbf{r} \rightarrow -\mathbf{r}$ does not preserve the structure ($\mathbf{r}$ is a position vector)], where the electron spin-degenerate parabolic bands split into dispersions with oppositely spin-polarized states. This effect can be illustrated via a relativistic electron in an asymmetric quantum well experiencing an effective magnetic field in its rest frame, induced by a perpendicular potential gradient ∇V, as represented by the spin-polarized momentum offset $\Delta k \propto \pm \nabla V$ (*18–21*). In terms of symmetries, the spin degeneracy associated with the spatial inversion symmetry is lifted due to a symmetry-breaking electric field normal to the heterointerface. Similar to the role of a potential gradient in the electronic Rashba effect, the space-variant orientation angle $\phi(x,y)$ of optical nanoantennas induces a spin-split dispersion of $\Delta k = \sigma \nabla \phi$ (*22–24*), where $\sigma_\pm = \pm 1$ is the photon spin corresponding to right and left circularly polarized light, respectively. We report on the design and fabrication of spin-optical metamaterial that gives rise to a spin-controlled dispersion due to the optical Rashba effect. The inversion asymmetry is obtained in artificial kagome structures with anisotropic achiral antenna configurations (Fig. 1, A and B) modeling the uniform ($q = 0$) and staggered ($\sqrt{3} \times \sqrt{3}$) chirality spin-folding modes in the kagome antiferromagnet (*25–27*). In the geometrically frustrated kagome lattice (KL), the reorder of the local magnetic moments transforms the lattice from an inversion symmetric (IS) to an inversion asymmetric (IaS) structure. Hence, we selected the KL as a platform for investigating the symmetry influence on spin-based manipulation of metamaterial dispersion.

It was previously shown that the localized mode resonance of an anisotropic void antenna

Micro and Nanooptics Laboratory, Faculty of Mechanical Engineering and Russell Berrie Nanotechnology Institute, Technion–Israel Institute of Technology, Haifa 32000, Israel.

*Corresponding author. E-mail: mehasman@technion.ac.il

Science

Multiscale Modeling of Membrane Rearrangement, Drainage, and Rupture in Evolving Foams

Robert I. Saye and James A. Sethian

Simulating Foam Formation

Foams are easily made whether in the kitchen sink in the form of soap bubbles or a frothy head on the top of a quickly poured beer. **Saye and Sethian** (p. 720; see the Perspective by **Weaire**) describe the mathematical simulation of foam dynamics by decomposing the process into rearrangement, drainage, and rupture phases that are then linked by coupling the flux boundary conditions.